# Growth generates a hyperdisordered pattern of chromatophores on squid skin

Robert J. H. Ross[1*], Giovanni D. Masucci[1], Chun Yen Lin[1], Teresa L. Iglesias[1], Sam Reiter[1*], Simone Pigolotti[1*]

[1]Okinawa Institute of Science and Technology, 1919-1 Tancha, Onna-son, Kunigami-gun, Okinawa, 904-0495, Japan.

*Corresponding author(s). E-mail(s): robert.ross@oist.jp; sam.reiter@oist.jp; simone.pigolotti@oist.jp;

**Abstract**

**Animal skin patterns take an astounding variety of forms, a result of dynamical processes at the cellular level acting as the organism grows. How cellular dynamics interact with organism growth to form skin patterns remains unclear. Here, we study this interplay by tracking the evolving cellular point pattern of chromatophores, the pigment cells present in squid skin. The arrangement of chromatophores appears locally ordered, but disordered at large spatial scales. In particular, its degree of disorder increases with spatial scale more rapidly than that of a purely random system. This atypical behaviour resembles highly irregular critical systems in statistical physics. We combine experiments and theory to reveal how this exotic pattern develops through chromatophore insertion as the organism grows. The mechanism we describe may apply to a broad class of growing tissues.**

## Main

In 1952, Turing proposed a mechanism explaining how patterns in a developing organism can be spontaneously generated through the interaction between two diffusing morphogens [1]. This groundbreaking idea paved the way for an understanding of patterns in living tissues. Over the years, alternative paradigms for pattern formation have been proposed, most notably the French-flag model, whereby a chemical gradient is used to establish a coordinate system [2]. These ideas have been pivotal for our

understanding of patterns in experimental model systems, including stripe formation in zebrafish [3], limb development [4], and fingerprint formation [5].

Many biological patterns are formed during growth. Modeling has shown that growth can substantially impact pattern formation. For example, growth can enhance its robustness [6], control selection [7, 8], and determine competition outcomes and population dynamics [9, 10]. However, experimental testing of these ideas has been limited, largely due to the difficulty in precisely measuring organism growth while simultaneously tracking the dynamics of pattern formation.

Some biological tissues present patterns which are composed of point-like units, such as hair follicles [11, 12], feather buds [13, 14], chromatophores [15], and photoreceptors [16]. These arrangements are referred to as "point patterns". Point patterns can be established by an eclectic range of processes. For instance, cell migration separates different cell types during development of the zebrafish retina [16]. Another mechanism is pre-patterning, whereby an initial process, for instance a Turing instability, lays a framework for a subsequent point pattern [12]. Typically, point patterns are shaped by exclusion zones, whereby cells maintain a minimum distance from each other [11, 13, 17].

Because of the prominent role of exclusion in determining biological point patterns, it is useful to draw an analogy with jammed physical systems, such as random collections of hard spheres at high density [18]. The degree of ordering of these patterns can be assessed by using tools from condensed and soft matter physics. Regular patterns would then correspond to crystals, whereas irregular patterns are analogous to liquid or glassy systems. However, one might expect behaviors in biological point patterns that go beyond those observed in physical systems, most prominently due to the role of tissue growth and the nature of the interactions between cells.

We sought to assess the impact of tissue growth on a point pattern. To this aim, we turned to the skin of the oval squid, *Sepioteuthis lessoniana*. *Sepioteuthis* grows rapidly, hatching with a mantle length of approximately 16mm and reaching 90mm within 3 months. Throughout development, its skin is populated by pigment-filled cells called chromatophores. Insertion of a chromatophore is thought to be possible only if the new chromatophore is at a minimum exclusion distance from preexisting ones [17, 19]. Following insertion into the skin, chromatophores do not move. This means that squid chromatophores, besides being the constitutive elements of a point pattern, can also function as reference points to precisely determine skin growth. To perform functions related to camouflage and communication, chromatophores can be expanded beyond their resting size through neurally controlled contraction of muscles surrounding each chromatophore [15]. However, throughout this work we used anaesthetised animals to focus exclusively on the resting size. A chromatophore's resting size (which we simply refer to as "chromatophore size" from now on) tends to increase as the chromatophore ages [20].

High-resolution images of squid mantles showed that chromatophores are arranged in a point pattern, characterized by larger chromatophores being surrounded by smaller ones (Fig. 1a, 1b). Visually, chromatophores appear at a characteristic distance

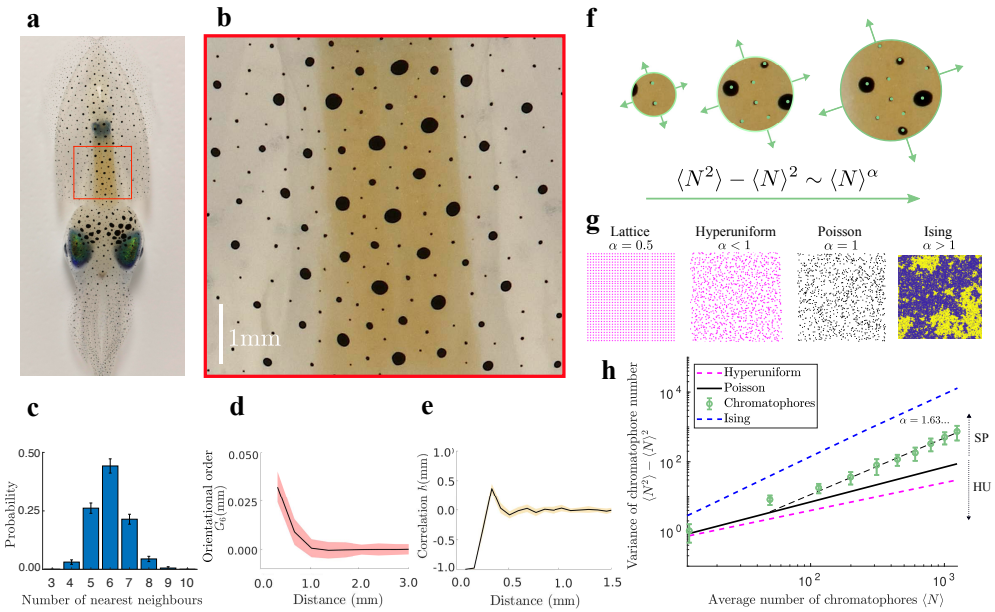


**Fig. 1 Chromatophores patterns are hyperdisordered. a** An approximately 6-weeks old squid, viewed from the top. **b** Magnification of the mantle region indicated by the red box in (a). **c** Histogram of nearest neighbours, computed via Delauney triangulation. **d** Orientational (hexatic) order as a function of distance to a chromatophore. **e** Spatial correlation of chromatophore position, as a function of distance to a chromatophore. (c-e: $N = 17140$ chromatophores from 10 squids). **f** Number of chromatophores $N$ sampled in circular areas of increasing radius $R$. **g** Examples of (left to right) a uniform pattern, a hyperuniform pattern, a Poisson pattern, and a configuration of the Ising model at the critical temperature. **h** Chromatophore number variance, as a function of chromatophore number within an expanding area for the synthetic patterns in (g), and for squid chromatophores, which show super-Poissonian scaling (SP).

from each other, forming a lattice-like structure. Quantitatively, the spatial density of chromatophores is consistent with a uniform distribution (Methods). Most chromatophores are surrounded by 6 neighbours, consistent with close packing, but with substantial variation in the distribution (Fig. 1c). The orientational (hexatic) order of nearby chromatophores [21], (Fig. 1d, SM Fig. 1a, 1b), as well as the correlation function (Fig. 1e), appeared to decay on a length scale comparable to the average inter-chromatophore distance ($0.29 \pm 0.05$ mm).

To directly characterize the degree of ordering of chromatophore patterns, we calculated how the number of chromatophores scales with the variance in the number of chromatophores (number variance) at increasing sample areas (Fig. 1f) [22]. For any spatially uniform pattern, the average number of points in a given sample area, $\langle N\rangle$, is proportional to the area. If points are independently placed at random, their number in each area follows a Poisson distribution, so that the number variance $\sigma_N^2 = \langle N^2\rangle - \langle N\rangle^2$ is proportional to the area as well. Combining these two relations, we find $\sigma_N^2 \propto \langle N\rangle$ for Poisson patterns. In regular lattices, the number variance grows

less than linearly with the area, so that, for large areas, the ratio $\sigma_N^2/\langle N\rangle$ tends to zero. The same property holds for maximally jammed systems, i.e. disordered systems that are so densely packed as to be mechanically rigid [22, 23]. These systems are collectively called hyperuniform (Fig. 1g).

Since chromatophore patterns (Fig. 1b) emerge through packed insertion into the skin, one may expect them to exhibit hyperuniform scaling. However, since the system is growing, small gaps are constantly being created between chromatophores, resulting in a loosely jammed system [17]. In fact, we observed that the number variance grows super-Poissonianly, i.e., more than linearly with $\langle N\rangle$ at large scales. We term this behavior "hyperdisordered". Hyperdisordered systems share some properties with critical physical systems, for example displaying large fluctuations at large scales. In fact, the Ising model, a paradigmatic example of a critical physical system, also presents hyperdisordered behavior (Fig. 1g). We are not aware of any previous example of hyperdisordered behavior in a biological pattern.

To elucidate the causes of this unconventional behaviour, we tracked a population of chromatophores on a growing patch of squid skin. We employed three-dimensional imaging to construct the skin manifold (Fig. 2a, SM Fig. 2a) and used computer vision techniques to segment chromatophores and locate their center of mass (Fig. 2b, Methods). Tracking an initial set of chromatophores over 6 weeks revealed a uniform linear growth in the inter-chromatophore distance over time, and consequently also in the system size (Fig. 2c). In parallel, individual chromatophores grew in size as they aged (Fig. 2b). Increases in chromatophore radii and separation were offset by the insertion of small new chromatophores into the skin, resulting in an approximately constant chromatophore density and stationary size distribution over time (Fig. 2d, 2e, and SM Fig. 2c, 3, 4).

These experimental results imply that chromatophores must grow in size at a pace that depends on the squid's age. To formalise this, we call $T_{\mathrm{sq}}$ the age of the squid, measured from the fertilization time of the egg (Fig. 3a). We also define the time $T_{\mathrm{exp}}$ elapsed from the first experimental observation, and the age $t_{\mathrm{chr}}^{(i)}$ of a given chromatophore, labeled by index $i$ (Fig. 3a). Given that the mantle grows linearly (Fig. 2c), our theory shows that if a chromatophore radius was solely a function of its age $t_{\mathrm{chr}}^{(i)}$, then the distribution of chromatophore radii would not be steady. We instead find that a steady distribution is achieved if chromatophore radii grow as a function of $\tau = T_{\mathrm{sq}}/(T_{\mathrm{sq}} - t_{\mathrm{chr}}^{(i)})$ (Methods). This means that the rate of chromatophore growth must slow down as the squid ages. In agreement with our theoretical prediction, we find that, at equal chromatophore ages, chromatophores that are born earlier tend to be larger (Fig. 3b). In contrast, when plotting chromatophore radii as a function of $\tau$, we obtain a precise collapse to a master curve (Fig. 3c). In this collapse, we treat $T_{\mathrm{sq}}$ as a free parameter, permitting us to estimate the value of $T_{\mathrm{sq}}$ corresponding to the start of the experiment, i.e., $T_{\mathrm{exp}} = 0$. This value is $T_{\mathrm{sq}} = 30.7$, which is consistent with the sum of the pre-hatching time (approximately 20 days) and the time between hatching and the beginning of our experiment (approximately 14 days). Further, by fitting individual chromatophore growth curves to the master curve, we estimate the

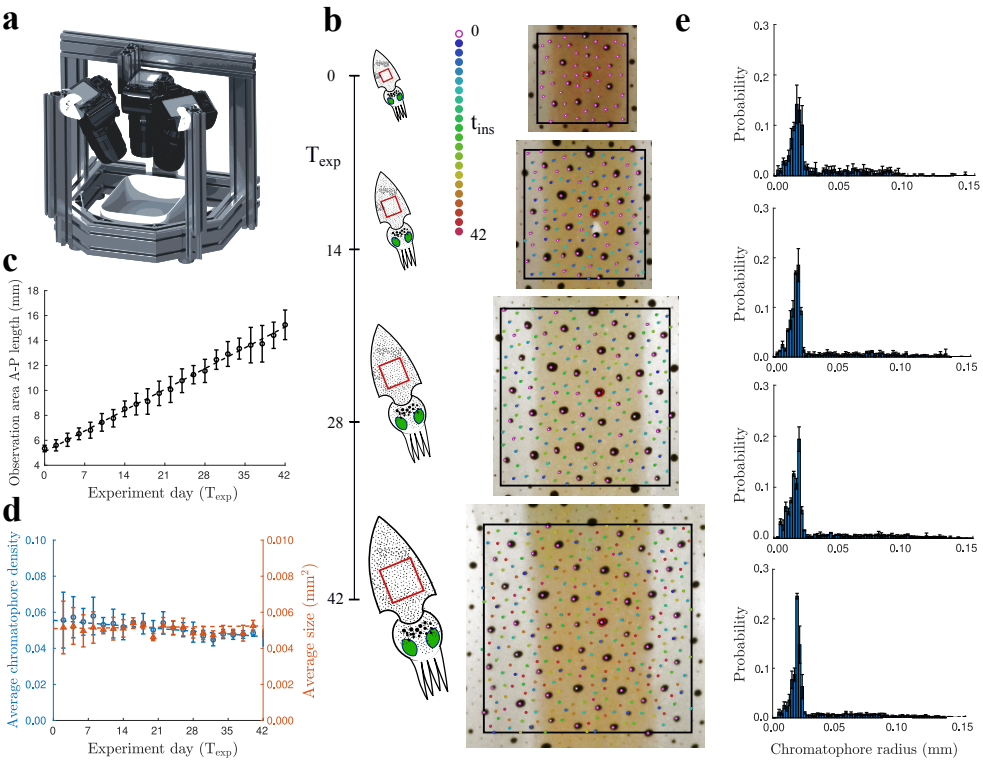


**Fig. 2 Chromatophore size distribution is maintained through a balance of cellular dynamics and surface growth a** Experimental setup for 3D imaging of squid skin. **b** Left: schematic of chromatophore tracking experiment. Right: skin patch with tracked chromatophores at experiment day ($T_{\text{exp}}$) 0, 14, 28 and 42. Color denotes chromatophore age (Methods). **c** Average observation area anterior-posterior length for three squids over 6 weeks. Dashed black line is linear fit to experimental data ($5.08 + 0.24\ T_{\text{exp}}$). **d** Average density and size of chromatophores in the observation area for three squids over 6 weeks. Dashed blue and orange lines are linear fit to correspondent experimental data ($0.05$ - $2 \cdot 10^{-4} T_{\text{exp}}$, and $5 \cdot 10^{-3} + 4 \cdot 10^{-6} T_{\text{exp}}$, respectively). **e** Distribution of chromatophore radii for day ($T_{\text{exp}}$) 0 ($N = 706$), 14 ($N = 1591$), 28 ($N = 2715$) and 42 ($N = 5029$) from 3 squids.

insertion date of chromatophores that appeared before the start of our observations (Fig. 3d, Methods). The complete distribution of chromatophore ages is well fitted by a quadratic law (Fig. 3e, $r^2 = 0.93$), although wave-like fluctuations are present for individual squids (SM Fig. 5). The predicted time for the appearance of the first chromatophore is $T_{\text{sq}} = 6.4$, which is consistent with the time of appearance of the first chromatophores on the unhatched squid after fertilization [24]. Thus, individual chromatophores reduce their growth rate as the squid ages in such a way that the distribution of chromatophore sizes is maintained steady during growth.

We now introduce a theoretical model to rationalize our experimental findings (Fig. 1h). In our model, chromatophores are inserted as the mantle grows linearly, with growth rate fit to experimental data (Fig. 4a). A chromatophore insertion is permitted

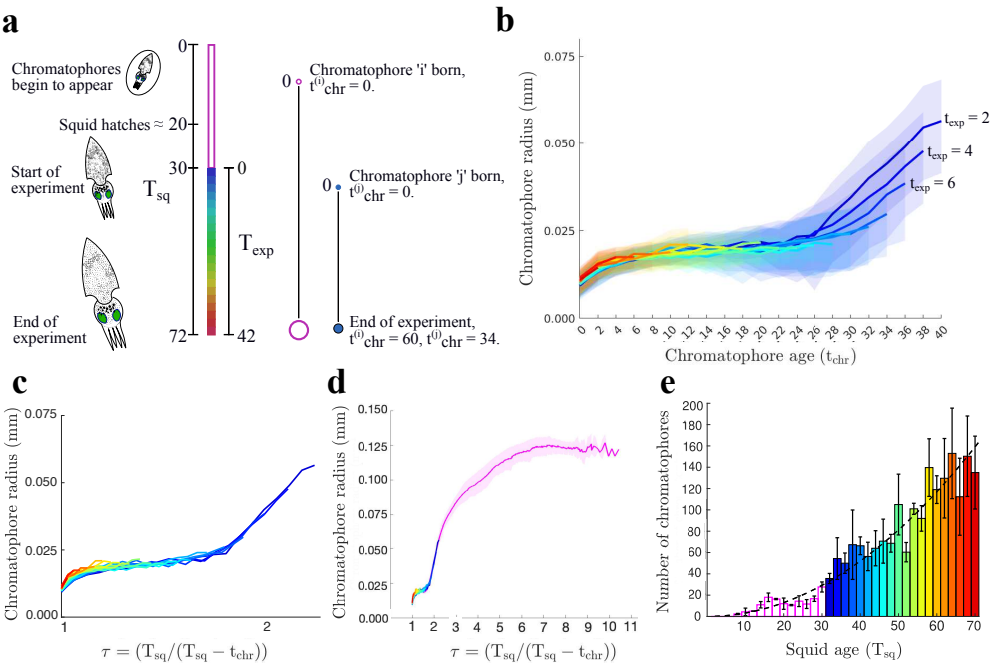


**Fig. 3 Chromatophore growth rate decays as the squid ages.** (a) Timeline of a squid development. We call $T_{\mathrm{sq}}$ the time measured from the fertilization of the squid egg, $T_{\mathrm{exp}}$ the time measured from the start of the experiment, and $t_{\mathrm{chr}}$ the age of a chromatophore. (b) Average evolution of chromatophore radii as a function of chromatophore age. Color denotes the experimental time, $t_{\mathrm{exp}}$, of chromatophore insertion ($N = 5733$ from 3 squids followed from approximately 2-weeks-old to 8-weeks-old). (c) Chromatophore radii plotted as function of $\tau$. (d) Average evolution of chromatophore radii as a function of chromatophore age with pre-experiment chromatophores included ($N = 6183$ from 3 squids). (e) Insertion times of all chromatophores. The black dashed line represent a quadratic fit.

only if the distance between the candidate new chromatophore and the existing ones is larger than an exclusion distance $\Delta$. This parameter is determined from the observed inter-chromatophore spacing (Fig. 1e and SM Fig. 2b,c). Chromatophore radii grow with a time-dependent rate which is also determined from experimental data (SM Fig. 6a, Methods). Based on experimental observations (see SM Fig. 2c), we assume that the exclusion distance $\Delta$ is independent of the chromatophore radius, i.e. the exclusion volume is not polydisperse.

Our model produces chromatophore patterns visually similar to those of real squids (Fig. 4b). Quantitatively, the distribution of number of neighbours (Fig. 4c, average number of nearest neighbours compared using a t-test, $p = 0.24$), the decay of the orientational order (Fig. 4d, expectation of distributions compared using a t-test, $p = 0.31$), and the correlation function (Fig. 4e, expectation of distributions compared using a t-test, $p = 0.74$) are consistent with experimental measurements. In particular, our simulation generates chromatophore patterns presenting hyperdisordered scaling of the number variance, similar to real squids (Fig. 4f). This scaling is robust with

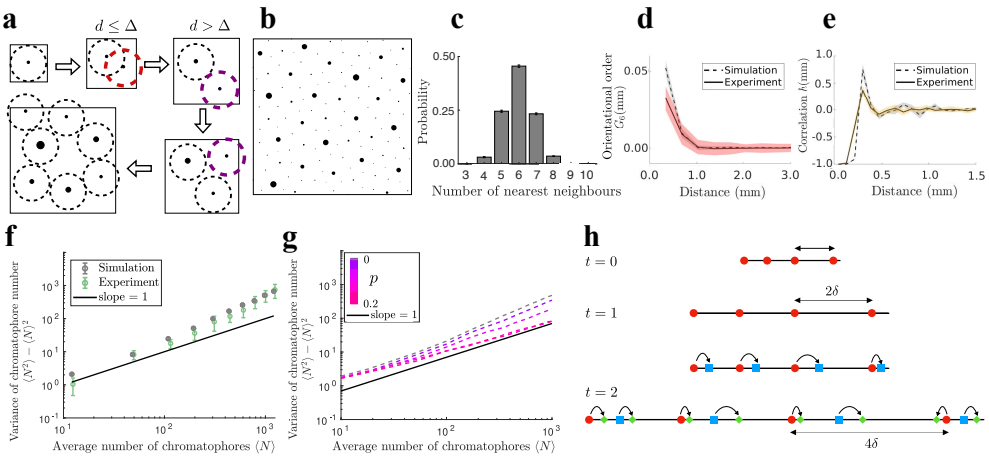


**Fig. 4 Growth generates hyperdisordered scaling.** (a) Schematic of simulation algorithm. The red dashed circle represents an event in which an attempted chromatophore insertion is rejected because the distance between chromatophore centres is too small. The purple dashed circle represents a successful chromatophore insertion. (b) A point pattern generated by the model. (c) Histogram of nearest neighbours, computed via Delauney triangulation. (d) Orientational order (hexatic). (e) Correlation function. (f) Number variance scaling. (g) A phase transition exists in polydispersion ($p$ is a polydispersion index defined as $p = \sqrt{\langle \epsilon^2 \rangle}$, where $\epsilon = ((a - \langle a \rangle)/\langle a \rangle)$, $a$ is the exclusion zone of a chromatophore (Methods and [25]). For c-g, $N = 5 \cdot 10^6$ chromatophores from 500 simulations. (h) Schematic of the 1D iterative model.

respect to the choice of initial condition (SM Fig. 7b). We have also verified that the occupied volume variance presents the same scaling as the number variance (SM Fig. 6e). Our model also reproduces the wave-like fluctuations present in the chromatophore age distribution (SM Fig. 6c,d). We interpret this behavior as a byproduct of jamming, whereby tissue growth creates space for new chromatophore insertion in an intermittent way. Taken together, these observations imply that chromatophore insertion at a fixed exclusion distance and tissue growth are sufficient ingredients to explain our experimental findings.

Theory shows that hyperdisordered behavior of a point pattern is necessarily associated with a pair correlation function whose integral in space diverges [23]. We verified that the envelope of the correlation function in our model decays approximately as $r^{-2}$ (SM Fig. 8d), so that its integral in space presents a logarithmic divergence in two dimensions. The pair correlation function in the squid is compatible with this power-law decay, within experimental error (SM Fig. 8c). The behavior of the structure factor (defined as the Fourier transform of the correlation function) is also consistent with hyperdisordered behaviour, both in the model and in the squid data (SM Fig. 8a and 8b).

A large-scale simulation of the model shows regularly packed domains with different densities and without a clear characteristic size, surrounded by other more disordered regions (SM Fig. 9). This heterogeneity is caused by the interplay between small-scale fluctuations and system growth. In a growing system like the squid mantle, density

fluctuations generated by insertion dynamics may be transported to ever larger scales through system growth, thus generating the observed hyperdisordered scaling. To test this idea, we studied a one-dimensional iterative model that recapitulates the essential features of our system. In this toy model, a set of chromatophores are arranged on a line. At each iteration of the model, $t$, the length of the line is doubled and new chromatophores are inserted next to existing ones, with a degree of randomness in their location (Fig. 4h). Our mathematical solution of this model shows that its behavior is generically hyperdisordered, independent of parameter values (Methods and SM Fig. 10).

We also used our model to explore how chromatophore patterns are affected by exclusion zones of variable size (polydispersion), focusing on zones that grow with chromatophore age (Methods). We found that the scaling of the number variance with the average number decreases with the degree of polydispersion, entering the hyperuniform phase only at large degrees of polydispersion (Fig. 4g). The occupied volume variance presents similar behavior, but with a larger parameter region in which the system is hyperdisordered (SM Fig. 6e). Taken together, these results show that monodispersion is not strictly required for hyperdisordered scaling, and that this scaling is robust to the method of measuring pattern behavior.

To conclude, we have demonstrated how growth affects squid chromatophore patterns by generating a hyperdisordered scaling of chromatophore number fluctuations. By combining experimental measurements and theory, we revealed that this unusual behavior spontaneously arises through the interaction of random packing and growth. In particular, growth is responsible for exporting short-range disorder generated by the packing process to ever larger spatial scales.

It is natural to speculate whether hyperdisordered scaling serves a biological purpose. One hypothesis is that this type of patterning facilitates the camouflage or communication functions of the squid skin display system. Indeed, it has been shown that systems displaying fluctuations on a broad range of scales are particularly efficient at processing complex environmental signals [26]. Further, recent work on plant morphogenesis has suggested that the exporting of fluctuations to large scales via growth may increase developmental robustness [27]. Alternatively, hyperdisordered scaling might be an evolutionary spandrel [28], i.e. a side effect of the interaction of growth and the regulation of a steady state density of chromatophores, traits which are themselves likely adaptive. A combination of these two hypotheses is also possible, whereby scaling emerged as a consequence of adaptive processes but was then co-opted to provide some additional benefit to the squid, i.e. exaptation [29]. The biological functions of pattern scaling behavior, unlike the general mechanism of pattern formation we describe, are likely to be system specific.

Additionally, we have found that the distribution of chromatophore sizes is maintained over time by slowing down the rate of chromatophore growth as the squid ages (Fig. 3). This result implies that chromatophores must possess some notion of the squid age during their growth. How this knowledge is acquired remains unclear. One possibility is that chromatophore growth rates are controlled by a morphogen

that scales with system size [30–32]. It is also possible that chromatophore growth is affected by other forms of biological aging.

We have shown that the hyperdisordered behavior we observed can be reproduced by a model using minimal ingredients: chromatophore insertion with an exclusion zone and simultaneous tissue growth. We therefore expect that this behavior might be observed in other growing biological or physical systems. In contrast, it has been observed that photoreceptors form a pattern on the chicken retina which possesses hyperuniform, rather than hyperdisordered, scaling properties [33]. It has been hypothesized that this behavior may provide optimal retinal coverage properties for vision. Based on these observations, we hypothesise that depending on the interaction of cell dynamics and tissue growth, biological point patterns can be funneled into different kinds of scaling behavior. Indeed, by altering the rules governing cell dynamics, our computational model is capable of producing a variety of patterns and corresponding scaling behaviours (see SM Fig. 7, 9).

Just as Turing's original idea shows that the interplay between reaction and diffusion can generate a variety of biological patterns, our work illustrates that the interplay of cell population dynamics and organism growth can unlock patterns that would be impossible in non-growing tissues. Given the ubiquity of this interplay in developmental biology, we expect this idea to extend far beyond our particular model system.

# References


[1] Turing, A. M. The chemical basis of morphogenesis. *Bulletin of mathematical biology* **52**, 153–197 (1952).

[2] Wolpert, L. Positional information and the spatial pattern of cellular differentiation. *Journal of theoretical biology* **25**, 1–47 (1969).

[3] Nakamasu, A., Takahashi, G., Kanbe, A. & Kondo, S. Interactions between zebrafish pigment cells responsible for the generation of turing patterns. *Proceedings of the National Academy of Sciences* **106**, 8429–8434 (2009).

[4] Raspopovic, J., Marcon, L., Russo, L. & Sharpe, J. Digit patterning is controlled by a bmp-sox9-wnt turing network modulated by morphogen gradients. *Science* **345**, 566–570 (2014).

[5] Glover, J. D. *et al.* The developmental basis of fingerprint pattern formation and variation. *Cell* **186**, 940–956 (2023).

[6] Crampin, E. J., Gaffney, E. A. & Maini, P. K. Reaction and diffusion on growing domains: scenarios for robust pattern formation. *Bulletin of mathematical biology* **61**, 1093–1120 (1999).

[7] Crampin, E. J., Hackborn, W. W. & Maini, P. K. Pattern formation in reaction-diffusion models with nonuniform domain growth. *Bulletin of mathematical*

*biology* **64**, 747–769 (2002).

[8] Krause, A. L., Ellis, M. A. & Van Gorder, R. A. Influence of curvature, growth, and anisotropy on the evolution of turing patterns on growing manifolds. *Bulletin of mathematical biology* **81**, 759–799 (2019).

[9] Ross, R. J., Yates, C. & Baker, R. E. Variable species densities are induced by volume exclusion interactions upon domain growth. *Physical Review E* **95**, 032416 (2017).

[10] Ross, R. J., Baker, R. E. & Yates, C. A. How domain growth is implemented determines the long-term behavior of a cell population through its effect on spatial correlations. *Physical Review E* **94**, 012408 (2016).

[11] Cheng, C. W. *et al.* Predicting the spatiotemporal dynamics of hair follicle patterns in the developing mouse. *Proceedings of the National Academy of Sciences* **111**, 2596–2601 (2014).

[12] Glover, J. D. *et al.* Hierarchical patterning modes orchestrate hair follicle morphogenesis. *PLoS biology* **15**, e2002117 (2017).

[13] Shyer, A. E. *et al.* Emergent cellular self-organization and mechanosensation initiate follicle pattern in the avian skin. *Science* **357**, 811–815 (2017).

[14] Yang, S. *et al.* Morphogens enable interacting supracellular phases that generate organ architecture. *Science* **382**, eadg5579 (2023).

[15] Messenger, J. B. Cephalopod chromatophores: neurobiology and natural history. *Biological Reviews* **76**, 473–528 (2001).

[16] Rocha-Martins, M. *et al.* Neuronal migration prevents spatial competition in retinal morphogenesis. *Nature* **620**, 615–624 (2023).

[17] Reiter, S. *et al.* Elucidating the control and development of skin patterning in cuttlefish. *Nature* **562**, 361–366 (2018).

[18] Conway, J. H. & Sloane, N. J. A. *Sphere packings, lattices and groups* Vol. 290 (Springer Science & Business Media, 2013).

[19] Packard, A. & Hochberg, F. Skin patterning in octopus and other genera **38**, 191–231 (1977).

[20] Packard, A. Squids old and young: Scale-free design for a simple billboard. *Optics & Laser Technology* **43**, 302–309 (2011).

[21] Halperin, B. & Nelson, D. R. Theory of two-dimensional melting. *Physical Review Letters* **41**, 121 (1978).

[22] Torquato, S. & Stillinger, F. H. Local density fluctuations, hyperuniformity, and order metrics. *Physical Review E* **68**, 041113 (2003).

[23] Torquato, S. Hyperuniform states of matter. *Physics Reports* **745**, 1–95 (2018).

[24] Samuel, V. D. & Patterson, J. Intercapsular embryonic development of the big fin squid sepioteuthis lessoniana (loliginidae) (2002).

[25] Berthier, L., Chaudhuri, P., Coulais, C., Dauchot, O. & Sollich, P. Suppressed compressibility at large scale in jammed packings of size-disperse spheres. *Physical review letters* **106**, 120601 (2011).

[26] Hidalgo, J. *et al.* Information-based fitness and the emergence of criticality in living systems. *Proceedings of the National Academy of Sciences* **111**, 10095–10100 (2014).

[27] Fruleux, A., Hong, L., Roeder, A. H., Li, C.-B. & Boudaoud, A. Growth couples temporal and spatial fluctuations of tissue properties during morphogenesis. *Proceedings of the National Academy of Sciences* **121**, e2318481121 (2024).

[28] Gould, S. J. & Lewontin, R. C. The spandrels of san marco and the panglossian paradigm: a critique of the adaptationist programme. *Conceptual Issues in Evolutionary Biology* **205**, 79 (1979).

[29] Gould, S. J. & Vrba, E. S. Exaptation—a missing term in the science of form. *Paleobiology* **8**, 4–15 (1982).

[30] Wartlick, O. *et al.* Dynamics of dpp signaling and proliferation control. *Science* **331**, 1154–1159 (2011).

[31] Averbukh, I., Ben-Zvi, D., Mishra, S. & Barkai, N. Scaling morphogen gradients during tissue growth by a cell division rule. *Development* **141**, 2150–2156 (2014).

[32] Aguilar-Hidalgo, D. *et al.* Critical point in self-organized tissue growth. *Physical review letters* **120**, 198102 (2018).

[33] Jiao, Y. *et al.* Avian photoreceptor patterns represent a disordered hyperuniform solution to a multiscale packing problem. *Physical Review E* **89**, 022721 (2014).

[34] Butler-Struben, H. M., Brophy, S. M., Johnson, N. A. & Crook, R. J. In vivo recording of neural and behavioral correlates of anesthesia induction, reversal, and euthanasia in cephalopod molluscs. *Frontiers in physiology* **9**, 326068 (2018).

[35] Woo, T. *et al.* The dynamics of pattern matching in camouflaging cuttlefish. *Nature* **619**, 122–128 (2023).

[36] Ronneberger, O., Fischer, P. & Brox, T. U-net: Convolutional networks for biomedical image segmentation 234–241 (2015).

[37] Bhattacharjee, S. M. & Seno, F. A measure of data collapse for scaling. *Journal of Physics A: Mathematical and General* **34**, 6375 (2001).

# Methods

## Experimental animals

All research and animal care procedures were carried out in accordance with institutional guidelines, approved by the OIST Animal Care and Use Committee under approval number 2019-244-6. Squids (*S. lessoniana*) were bred in the OIST Marine Science Station. Juvenile squids used for this study were group housed in 50x40x40cm tanks connected to the ocean through an open seawater circulation system.

## Chromatophore imaging

For the analysis presented in Fig. 1, 10 animals (8 weeks post-hatching) were anesthetized (1 percent ethanol [34]), and individually transferred to a filming chamber for approximately 1 minute (Fig. 2a). They were photographed using a high resolution camera ($8688 \times 5792$ pixels, approximate pixel size $7\mu$m $\times$ $7\mu$m). After imaging, animals were transferred to filtered seawater, and returned to their home tank after waking from anesthesia.

## Data acquisition for chromatophore tracking

For chromatophore tracking, 12 animals (2-3 weeks post-hatching) were photographed in three dimensions using a 3-camera rig (Fig. 2a). Image acquisition was synchronized via an Arduino. Cameras were calibrated using a checkerboard (square size = 5mm $\times$ 5mm), and the reprojection error was typically less than a pixel. Images were taken every 2 days for 42 days. Squid identity was maintained across days using the spatial arrangement of chromatophores.

## Summary of the image processing and tracking procedure

Within an image, chromatophore locations were determined through segmenting chromatophores using a U-net [35, 36], followed by image binarization and centroid detection. These locations were manually curated via visual inspection.

For multi-camera imaging, points corresponding to chromatophore centroids were matched through nonlinear warping of pairs of images using a custom GUI [35], followed by nearest-neighbour association of points across the two images. With chromatophore centroids identified across simultaneously acquired images, the three-dimensional location of chromatophores within a day was determined using the camera calibration. Chromatophores were tracked across days in a similar manner, using nonlinear warping and nearest-neighbor matching between images separated by 2 and 4 days. A chromatophore was labelled as new if it did not have a corresponding chromatophore from the previous 2 and 4 day images.

## Uniformity of the spatial distribution of chromatophores

Equally sized images of chromatophores were divided into 16 equally sized sections and the number of chromatophores in each box was compared to both the expected number of chromatophores within an image, and across all images (N = 10), using a $\chi^2$ test. The null hypothesis, that chromatophores were present in equal proportions across sections, was not rejected in all cases at significance level $\beta = 0.05$. We conclude that the spatial distribution of chromatophores is uniform, within our experimental uncertainty.

## Condition for steady chromatophore size distribution

Here, we derive the condition for a steady distribution of chromatophore sizes. Since the density of chromatophore sizes is approximately constant during growth, the total number of chromatophores is proportional to the mantle area, which in turn grows as the square of the squid age (linear growth). This means that $N(T_{\mathrm{sq}}) \propto T_{\mathrm{sq}}^2$. The distribution of chromatophore ages for $T_{\mathrm{sq}} \gg 1$ is proportional to $\dot{N}(T_{\mathrm{sq}} - t_{\mathrm{chr}})$, i.e., how many chromatophores were inserted at time $(T_{\mathrm{sq}} - t_{\mathrm{chr}})$. After normalization, we conclude that the distribution of chromatophore ages, for large $T_{\mathrm{sq}}$, is expressed as $2(T_{\mathrm{sq}} - t_{\mathrm{chr}})/T_{\mathrm{sq}}^2$.

We call $p(R|t_{\mathrm{chr}}, T_{\mathrm{sq}})$ the probability that a chromatophore has radius $R$, given its age $t_{\mathrm{chr}}$ and the squid age $T_{\mathrm{sq}}$. If the radius is uniquely determined by these two quantities, this probability is given by a delta function. We similarly define the probability $p(R)$ that a randomly chosen chromatophore has radius $R$. We obtain

$$p(R) = \int_0^\infty dt_{\mathrm{chr}}\, p(R|t_{\mathrm{chr}}) \frac{2(T_{\mathrm{sq}} - t_{\mathrm{chr}})}{T_{\mathrm{sq}}^2}. \tag{1}$$

If $p(R|t_{\mathrm{chr}}, T_{\mathrm{sq}})$ did not depend on $T_{\mathrm{sq}}$, then Eq. (1) would predict that $p(R)$ would not be stationary. This proves that aging is necessary for achieving a steady size distribution. If, instead, $R$ is a deterministic function of $\tau = T_{\mathrm{sq}}/(T_{\mathrm{sq}} - t_{\mathrm{chr}})$, then the distribution $p(R)$ would always be stationary. This result can be verified by directly substituting $p(R|t_{\mathrm{chr}}) = \delta(R - f(\tau))$ into Eq. (1), where $f(\tau)$ is an arbitrary increasing function. Corresponding plots and additional results can be found in SM Fig. 11.

## Kolmogorov-Smirnov test for comparing chromatophore radius distribution through time

Chromatophore radius data was pooled from 3 squids and binned into equally-sized bins $(0, 0.01, 0.02, ..., 0.18)$ for each $T_{\mathrm{exp}} \in (0, 2, 4, ..., 42)$. We then performed two separate analyses using these distributions: (1) each $T_{\mathrm{exp}}$ was compared to the distribution made by aggregating chromatophore radii data across all times, (2) each $T_{\mathrm{exp}}$ was compared individually against all other $T_{\mathrm{exp}}$. In the case of (1), from 22 tests the null hypothesis was rejected 3 times at $\beta = 0.05$. In the case of (2), from 231 tests the null hypothesis was rejected 27 times, also at $\beta = 0.05$. This means for both analyses the null hypothesis was not rejected in approximately 85% of cases. Therefore, we assume the chromatophore size distribution is steady.

## Inference of chromatophore insertion times

New chromatophores were pooled for each $T_{\text{exp}} \in (0, 2, 4, ..., 42)$ across 3 squids to generate the chromatophore trajectories in Fig. 3 (b). $T_{\text{sq}}$ at $T_{\text{exp}} = 0$ was determined by minimising the residuals between chromatophore trajectories according to the function $T_{\text{sq}}/(T_{\text{sq}} - t_{\text{chr}})$. This resulted in $T_{\text{sq}} = 30.7$ days. The corresponding trajectories are displayed in Fig. 3 (c). From these trajectories a master curve was generated using MATLAB's curve-fitting tool box (see below for function) and the residuals of remaining chromatophores whose size coincided with this master curve were minimised using an interpolation scheme [37]. Following this procedure, a new master curve was generated, and the residuals of remaining chromatophores whose size coincided with this master curve were minimised. This process was iterated until all remaining chromatophores had been matched. The final master curve is displayed in SM Fig. 6a.

## Chromatophore growth function

The function describing the growth of the chromatophore radius with respect to $\tau$ was fitted to a $5^{th}$ degree rational using MATLAB's curve-fitting toolbox. The equation is:

$$R(\tau) = \frac{(p_1\tau^5 + p_2\tau^4 + p_3\tau^3 + p_4\tau^2 + p_5\tau^1 + p_6)}{(\tau^5 + q_1\tau^4 + q_2\tau^3 + q_3\tau^2 + q_4\tau^1 + q_5)}, \tag{2}$$

and the initial size of a chromatophore $R(1) = c_r = 1.25 \cdot 10^{-2}$. The coefficient values are given in Table 1. The support for this function is $\tau \in [1, 7.55]$. For $\tau > 7.55$, we

**Table 1** Coefficient values

| | |
|---|---|
| $p_1$ | 0.15 |
| $p_2$ | -2.21 |
| $p_3$ | 11.95 |
| $p_4$ | -27.98 |
| $p_5$ | 28.77 |
| $p_6$ | -10.25 |
| $q_1$ | -13.09 |
| $q_2$ | 56.39 |
| $q_3$ | -67.27 |
| $q_4$ | -50.63 |
| $q_5$ | 108.4 |

implement a linear function

$$R(\tau) = c_{r2} + 2.42 \cdot 10^{-4}\tau,$$

where $c_{r2} = R(7.55) = 0.126$. Eq. (2) is plotted in the SM Fig. 6a.

## Squid model

We here provide details on our model of chromatophore point pattern formation. Chromatophore insertion is attempted by drawing new coordinate pairs ($x_{\text{new}}$, $y_{\text{new}}$) uniformly and at random, from within the current domain. Chromatophore insertion is successful if

$$(x_{\text{new}} - x_i)^2 + (y_{\text{new}} - y_i)^2 > \Delta^2 \qquad \forall i, \tag{3}$$

where $(x_i, y_i)$ are the coordinates of an existing chromatophore $i$ and the parameter $\Delta$ is the exclusion distance, i.e., the minimum distance between chromatophore centers. Otherwise, the attempt is discarded.

During the simulation, chromatophore insertions are repeatedly attempted, until a maximum number of sequential failures is reached. Once this occurs, the domain length in both the $x$ and $y$ direction is increased by $P_d \cdot dt$, where $P_d$ is the domain growth rate and $dt$ is the simulation time step. In this growth step, the coordinates of all chromatophores are rescaled proportionally to the new domain size. Chromatophore insertion is again attempted until the maximum number of sequential failures is reached. The maximum number of sequential failures $f$ is increased linearly in time throughout the simulation.

To include polydispersion in the model the exclusion zone of chromatophore $i$ is defined as $a = 0.5\Delta + \gamma R(\tau)$. $\gamma = 0$ is the monodisperse model, and $\gamma = 1$ is approximately $p = 0.2$. The other values present in Fig. 4g are $\gamma = 0.1$, 0.25, and 0.5.

All simulations were written in C++ and run on the supercomputer Deigo at OIST.

## Parameters of the squid model

The exclusion distance is set to $\Delta = 0.25$ mm, based on experimental data (see SM Fig. 2). The initial domain area is $1.5\Delta \times 1.5\Delta$. We explored a range of initial areas (Fig. 4 g). The domain linear growth rate is $P_d = 0.24$ mm per day (see Fig. 2). The number of failed insertion attempts before advancing time by a timestep is increased quadratically. The initial simulation time is $t = T_{\text{start}} = 6.4$ days, in accordance with the time of first appearance of chromatophores inferred from experimental data (see Fig. 3). The timestep is set to $dt = 10^{-3}$days.

## Iterative model

In the iterative model, a 1D domain is initialised with $\nu$ cells placed uniformly at random. In analogy with the squid model, we call $\Delta$ the typical distance between cells. In all simulations $\Delta = 1$, so that an initial domain of integer length $L$, contains $n = L$ initial cells. At each step of the model, the domain size is doubled and new cells are placed at $x_i + \mathcal{N}(\Delta, \gamma)$, where $x_i$ are the positions of the cells already present and $\mathcal{N}$ is a Gaussian random variable with mean $\Delta$ and variance $\gamma$. This process is repeated for $t$ steps, so that the final domain size is $n \times 2^t$.

The structure factor of the initial condition is defined by

$$S_0(k) = \frac{1}{n} \sum_{i,j=1}^{n} \left\langle e^{ik(x_i - x_j)} \right\rangle . \tag{4}$$

A point pattern is hyperdisordered if the structure factor diverges as $k \to 0$. We find that the structure factor of the iterative model is expressed as

$$S_t(k) = 2^t S_0(2^t k) \prod_{i=1}^{t} F(2^{t-i}k) + \sum_{i=1}^{t} 2^{t-i}\phi(2^{t-i}k) \prod_{j=1}^{t-i} F(2^{t-i-j}k), \tag{5}$$

where

$$F(k) = \frac{1}{4}\left(1 + 2\cos(\Delta k)e^{-\frac{k^2\sigma^2}{2}} + e^{-k^2\sigma^2}\right), \tag{6}$$

and

$$\phi(k) = \frac{1}{2}\left(1 - e^{-k^2\sigma^2}\right), \tag{7}$$

see the SM for a derivation. For large $t$, the structure factor given in Eq. (5) diverges for $k \to 0$ (see SM), meaning that the behavior of the iterative model is hyperdisordered, regardless of the parameter choice.

## Statistics

Unless stated otherwise, data are mean ± standard deviation.

## Data availability

Data are available from the corresponding authors on request.

## Code availability

The code used in this paper can be found in GitHub repository [].


## Acknowledgements

We are grateful to the OIST Cephalopod Research Support Team for animal care, for the help and support provided by the Scientific Computing and Data Analysis and Engineering sections, Research Support Division at OIST. We thank all Pigolotti and Reiter laboratory members for assistance and discussion. We thank Mahesh Bandi, Joshua Shaevitz, and Salvatore Torquato for feedback on a preliminary version of this manuscript.


## Author contributions

The project was defined by R.R., S.R., and S.P. Experiments and data analysis was performed by R.R. and S.R. Modeling and theory was performed by R.R. and S.P. Animal care was performed by G.M., C.L.L., and T.I. The manuscript was written by R.R., S.R., and S.P.

## Competing interests

The authors declare no competing interests.